2. Materials and methods

2.1. Generation of Rnf213 knockout mice

An *Rnf213*-targeting construct was produced using a Multisite Gateway Three-Fragment Vector Construction Kit (Invitrogen). Briefly, a loxP site was cloned into the 5′ site of exon 20, and a fragment containing a loxP site and a neomycin-resistance gene (Neo) was cloned into the 3′ site of exon 20 (Fig. 1A, Supplemental material). The construct was linearized and electroporated into RENKA C57BL/6 ES cells and selected with G418. Integration of the targeting vector into the mouse genome by homologous recombination was verified in targeted ES clones by Southern blotting (data not shown). Correctly targeted clones were injected into C57BL/6 blastocysts to generate chimeric mice with the targeted allele incorporated into the germ lines. The resulting chimeric male mice were mated with female C57BL/6 mice, and germ line transmission of the targeted allele was examined in the offspring. Offspring carrying the target allele were bred with Cre-transgenic C57BL/6 mice to generate mice heterozygous for the *Rnf213* deficiency ($Rnf213^{-/+}$). Heterozygous male and female mice were bred to produce homozygous offspring (KO, $Rnf213^{-/-}$).

2.2. Experimental animals

Akita ($Ins2^{+/C96Y}$) mice on a C57BL/6 background and C57BL/6 (WT) mice were purchased from Japan SLC. To generate mice lacking *Rnf213* and carrying the Akita mutation (KO/Akita, $Rnf213^{-/-}$; $Ins2^{+/C96Y}$), male double-heterozygous ($Rnf213^{+/-}$; $Ins2^{+/C96Y}$) mice were generated and mated with female *Rnf213* KO mice. Experiments were performed on four groups of male mice: (1) KO/Akita ($Rnf213^{-/-}$; $Ins2^{+/C96Y}$), (2) Akita ($Rnf213^{+/+}$; $Ins2^{+/C96Y}$), (3) KO ($Rnf213^{-/-}$; $Ins2^{+/+}$), and (4) WT ($Rnf213^{+/+}$; $Ins2^{+/+}$). Progeny of (1–3), aged 4 weeks, were selected by PCR genotyping for *Rnf213* (Supplemental material) and the *Ins2* locus, as described [13]. Mice were allowed free access to a standard diet (CLEA, Rodent Diet CE-7, 3.4 kcal/g) and tap water. The care of the animals and all experimental procedures were in accordance with the Animal Welfare Guidelines of Kyoto University.

2.3. Culture of Akita and min-6 cell lines and real-time PCR (RT-PCR)

To test *Rnf213* expression in β cells, we used Akita cells and the min-6 cell line [14,15]. Quantitative RT-PCR for *Rnf213* was performed using the specific primers, Rnf213cex29–31F (5′-TAA GGA TGT CCG CTC CTG GTT-3′) and Rnf213cex29–31R (5′-TTG ATG GCA GTA TAC TTG GCA-3′).

2.4. Western blotting

Protein samples from mice pancreas or cultured cells were subjected to immunoblotting using the rabbit polyclonal anti-RNF213 antibody and anti-GAPDH antibody (Santa Cruz Biotechnology). The rabbit polyclonal antibody was produced by inoculation of rabbits with cloned human full-length RNF213 as an antigen. The polyclonal IgG was purified from rabbit serum.

2.5. Measurement of glucose, insulin, proinsulin and leptin

Blood glucose was measured by Glutest Neo Super (Sanwa). All values above 600 mg/dl were treated as 600 mg/dl. Glucose tolerance testing (GTT) was performed by fasting 18-week-old mice for 16 h, followed by an intraperitoneal injection of 1.5 g/kg glucose. Insulin tolerance testing (ITT) was performed by fasting 18-week-old mice for 6 h, followed by an intraperitoneal injection of 1.5 U/kg insulin (Eli Lilly and Company). To measure leptin concentrations, blood was collected from the tail veins of 18-week-old mice after a 16 h fast. Plasma concentrations of insulin, leptin and proinsulin were measured by ELISA (Shibayagi).

2.6. Measurement of pancreatic insulin and proinsulin contents

Mice were sacrificed at 18 weeks of age in the morning after a 6 h fast. Each pancreas was homogenized in acid ethanol (75% ethanol, 1.5% HCl) and extracted at 4 °C overnight. The extracts were centrifuged, and the insulin and proinsulin concentrations of the supernatants were measured.

2.7. Pathological investigations

Mice were sacrificed under sevoflurane at 18 weeks of age after a 6 h fast. Each pancreas was fixed in 10% formaldehyde, embedded in paraffin, and sectioned. The sections were immunostained with guinea pig anti-insulin antibody (Dako) or rabbit anti-C/EBP homologous protein (CHOP)/GADD153 antibody (Santa Cruz Biotechnology). To estimate β-cell mass, consecutive paraffin sections 75 μm apart and spanning the entire pancreas (5–8 sections per pancreas) were prepared, and islet areas and relative abundance of insulin- and CHOP-positive cells were quantified on more than 20 islets per pancreas in three or four mice per genotype using Image-J software (National Institutes of Health). For electron microscopy, pancreases were fixed in 2% glutaraldehyde and post-fixed in 1% osmium tetroxide.

2.8. Statistical analysis

Results are presented as the mean ± standard deviation (SD) or standard error (SE). Differences were analyzed by *t*-test or ANOVA followed by Tukey's honestly significant difference test using STATISTICA software (StatSoft). $p < 0.05$ was considered statistically significant.

3. Results

3.1. General characterization of Rnf213 KO mice

To determine the physiological function of *Rnf213*, we generated mice with targeted deletion of *Rnf213* exon 20. This targeting strategy, in which a frame shift mutation was introduced into this exon, resulted in the disruption of the Walker motifs and the ring finger domain (Fig. 1A). Complete removal of *Rnf213* exon 20 from genomic DNA (Fig. 1B) and the absence of Rnf213 protein expression (Fig. 1C), were confirmed in KO mice. KO mice were born in the predicted Mendelian ratio and did not show any apparent health problems, including a cerebrovascular phenotype similar to MMD, even at around 80 weeks of age. Both males and females were fertile and produced normal-sized litters (mean, 6–8 pups). The body weight of KO mice was about 13% less than that of WT mice after 25 weeks of age ($p < 0.05$), and GTT results in KO and WT mice did not differ at 50 weeks of age (Supplemental Fig. 1).

3.2. Expression of Rnf213 in Akita and min-6 cells

Rnf213 protein was expressed in the pancreas (Fig. 1C). To assess the expression of *Rnf213* in β cells, we investigated the expression of *Rnf213* mRNA and protein in Akita and min-6 cell lines by quantitative RT-PCR and western blotting, respectively. We found that *Rnf213* mRNA and protein were expressed in these cells, with no differences between Akita and min-6 cell lines (Fig. 1D and E).

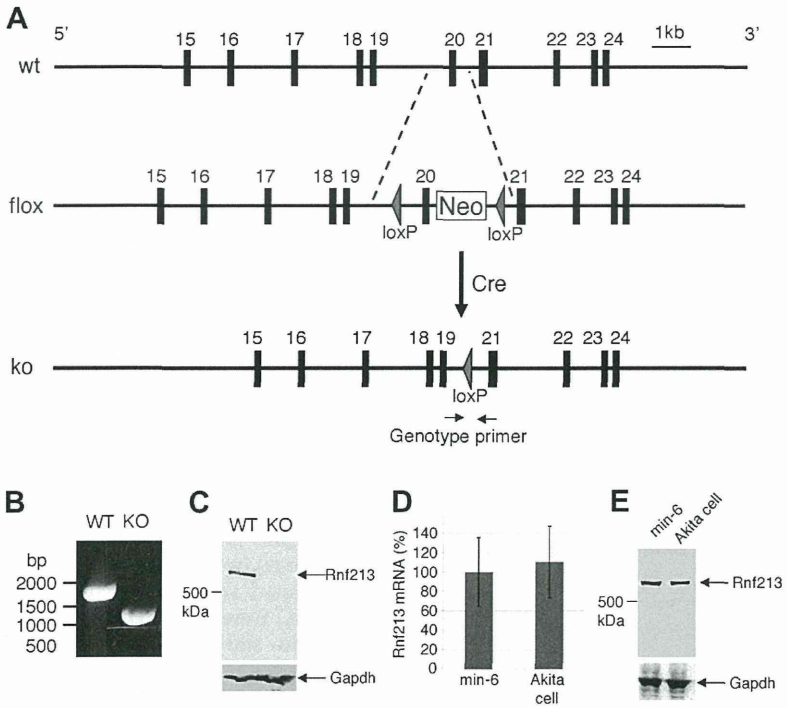

Fig. 1. Generation of *Rnf213* KO mice. (A) Structure of the endogenous mouse *Rnf213* gene, the targeted allele, and the disrupted allele. (B) PCR genotyping of WT and KO mice. (C) *Rnf213* immunoblotting of pancreas extracts from WT and KO mice. (D) Quantitative RT PCR for *Rnf213* in Akita and min-6 cells. Data are shown as mean ± SD. (E) *Rnf213* immunoblotting of extracts from Akita and min-6 cells. Membranes were immunoblotted with antibody to GAPDH as a loading control.

3.3. Body weight over time

The mean body weight of KO/Akita mice was lower than that of Akita mice between 6 and 9 weeks of age, although they did not differ after 10 weeks of age (Fig. 2A). The mean body weights of both KO/Akita and Akita mice were significantly lower than those of KO and WT mice. Between 6 and 20 weeks of age, there were no differences in body weight between KO and WT mice.

3.4. Blood glucose level and glucose tolerance

From 6 to 20 weeks of age, blood glucose concentrations after a 16 h fast were consistently and significantly lower in KO/Akita than in Akita mice (Fig. 2B). Moreover, blood glucose levels after a 6 h fast were significantly lower in 18 week old KO/Akita (348 ± 153 mg/dL) than in Akita (572 ± 42 mg/dL) mice, although both were significantly higher than in KO (140 ± 32 mg/dL) and WT (147 ± 22 mg/dL) mice (Fig. 2C). GTT at 18 weeks showed that glucose tolerance in KO/Akita (Area under the curve [AUC] 49298 ± 8864 mg min/dL) mice was impaired relative to KO (AUC 22179 ± 1516 mg min/dL) and WT (AUC 18284 ± 1170 mg min/dL) mice, but was better than in Akita mice (AUC 62346 ± 9105 mg min/dL) (Fig. 2D and E). These results indicated that deletion of *Rnf213* led to improvements in glucose tolerance in Akita mice. We also investigated the insulin sensitivity of KO/Akita mice. ITT at 18 weeks of age revealed no difference in insulin sensitivity among the KO/Akita, Akita, KO and WT strains (Fig. 2F).

3.5. Plasma insulin and proinsulin concentrations

Plasma insulin concentrations were significantly higher in 18 weeks old KO/Akita (1300 ± 270 pg/mL) than in Akita mice (54 ± 14 pg/mL) after a 6 h fast, but were similar in KO/Akita, KO (1466 ± 323 pg/mL) and WT (783 ± 93 pg/mL) mice (Fig 3A). Plasma insulin concentrations after fasting for 6 h and 16 h showed a significant and positive correlation with blood glucose concentrations in KO/Akita ($R = 0.50$, $p = 0.0009$), but not in Akita ($R = 0.26$, $p = 0.275$), mice (Fig. 3B), indicating that insulin secretion was responsive to increased blood glucose in KO/Akita, but not in Akita, mice. The plasma ratios of proinsulin/insulin concentrations did not differ significantly among KO/Akita, KO and WT mice (Supplemental Fig. 2A). Proinsulin was not detected in the plasma of Akita mice.

3.6. Food intake and plasma leptin concentration

Male Akita mice develop more profound diabetes than female Akita mice. Castration of male Akita mice alleviated such sex differences by reducing hyperphagia [16]. We have shown that castration normalized hyperphagia by acting on plasma leptin and normalizing anorexigenic proopiomelanocortin (POMC) [16]. To examine the regulation of feeding, we measured food consumption and plasma leptin concentration. Food consumption by KO/Akita mice (3.92 ± 0.78 g/day) was similar to that by KO (3.25 ± 0.33 g/day) and WT (3.06 ± 0.23 g/day) mice, but was 34% lower than by Akita mice (5.96 ± 0.68 g/day) (Fig. 3C). Plasma leptin concentrations were similar in KO/Akita (353 ± 226 pg/mL) and Akita (348 ± 43 pg/mL) mice, but lower than in KO (741 ± 156 pg/mL) and WT (744 ± 145 pg/mL) mice (Fig. 3D), suggesting that decreased food consumption in KO/Akita mice was likely attributable to elevated insulin concentration, which stimulates overlapping insulin-leptin signal pathways in the central nervous system to suppress appetite [17].

3.7. Pancreatic insulin and proinsulin concentration

Total pancreatic insulin levels were significantly higher in KO/Akita (2689 ± 746 ng/pancreas) than in Akita (1102 ± 43 ng/pancreas) mice, although they were about one-fifth of those in KO (14,434 ± 3359 ng/pancreas) and WT (13,348 ± 2500 ng/pancreas) mice (Fig. 4A). Pancreatic proinsulin contents were also signifi-

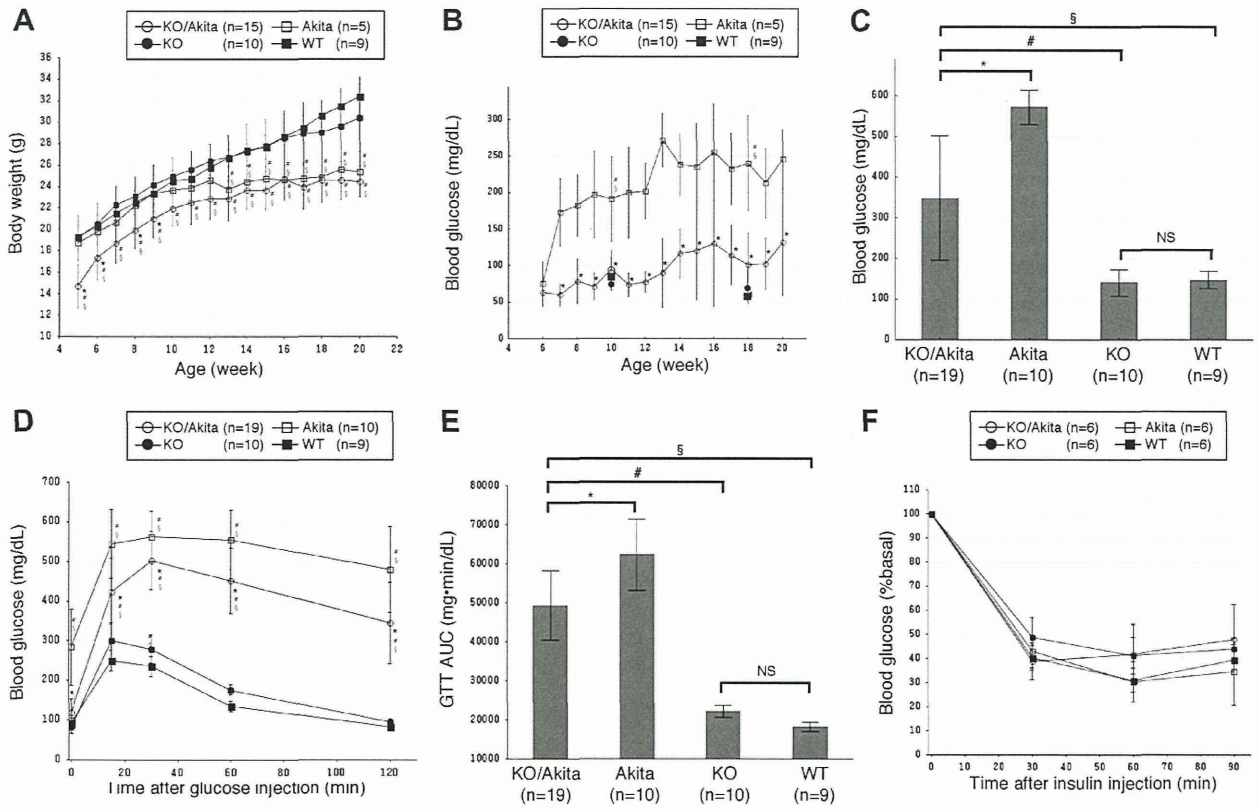

Fig. 2. Mouse growth curves, blood glucose concentrations, GTT and ITT. (A) Time course of body weight of KO/Akita, Akita, KO, and WT mice from 6 to 20 weeks of age. (B) Time course of 16 h fasting blood glucose concentrations in KO/Akita, Akita, KO and WT mice from 6 to 20 weeks of age. Glucose concentrations in KO and WT mice were measured at 10 and 18 weeks of age. (C) Six hours fasting blood glucose concentrations in 18 week old KO/Akita, Akita, KO, and WT mice. (D and E) GTT of 18 week old KO/Akita, Akita, KO, and WT mice. Blood glucose concentrations are shown at indicated times after glucose injections. Area under the curve was calculated for these mice. (F) ITT in 18 week old KO/Akita, Akita, KO, and WT mice. Blood glucose concentrations are shown at indicated times after insulin injections. Data are shown as mean ± SD. $^{*}p < 0.05$ vs Akita, $^{\#}p < 0.05$ vs KO, $^{\S}p < 0.05$ vs WT, NS, Not significant.

cantly higher in KO/Akita than in Akita mice (Supplemental Fig. 2B). Pancreas weight was similar in these 4 groups (Supplemental Fig. 3A).

3.8. Immunohistochemical assays of insulin and CHOP, and electron microscopy of islets

No morphological abnormalities were observed in the pancreas or islets of KO/Akita and KO mice. Immunohistochemical examination showed that a higher proportion of insulin-positive β cells was preserved in the islets of KO/Akita (0.141 ± 0.046 insulin positive cells/islet) than of Akita (0.088 ± 0.042 insulin positive cells/islet) mice, although both were lower than in KO (0.643 ± 0.080 insulin positive cells/islet) and WT (0.616 ± 0.076 insulin positive cells/islet) mice (Fig. 4B). Mean islet area did not differ among KO/Akita, Akita, KO and WT mice (Supplemental Fig. 3B).

CHOP is an ER stress-inducible transcription factor that promotes apoptosis [18] and that has been used as a marker of ER stress-mediated apoptosis in β cells of Akita mice [19]. To test whether ER stress occurs in the β cells of KO/Akita mice, we assayed for CHOP immunohistochemically. The percentage of CHOP-positive cells in islets was significantly lower in KO/Akita (0.102 ± 0.042 CHOP positive cells/islet) than in Akita (0.135 ± 0.037 CHOP positive cells/islet) mice, but were much lower in KO (0.002 ± 0.000 CHOP positive cells/islet) and WT (0.002 ± 0.000 (CHOP positive cells/islet) mice (Fig. 4C), indicating that ER stress is lower in the β cells of KO/Akita mice.

Electron microscopy of β cells in WT mice revealed abundant mature secretory granules in the cytoplasm, inconspicuous ER, and intact mitochondria with cristae (Fig. 4D, WT). KO mice showed no morphological abnormalities (Fig. 4D, KO). In contrast, examination of Akita mice showed a small number of secretory granules, a tubulovesicular structure comprised of markedly enlarged ER, and swelling or disruption of mitochondria (Fig 4D, Akita), indicators of insulin secretory pathway impairment and ER stress. Unlike Akita mice, KO/Akita mice showed mild ER enlargement and slight swelling of the mitochondria in β cells, although the number of secretory granules was markedly reduced (Fig. 4D, KO/Akita), suggesting less ER stress in the β cells of these mice than in Akita mice. The α cells of KO/Akita, Akita, KO and WT mice were morphologically similar (data not shown).

4. Discussion

We have shown here that targeted disruption of *Rnf213* unexpectedly improved glucose tolerance in Akita mice, although insulin sensitivity was not altered. These findings are consistent with results showing that plasma and pancreatic insulin levels were higher in KO/Akita than in Akita mice. Moreover, disruption of *Rnf213* reduced hyperphagia by elevating plasma insulin concentrations in KO/Akita, but did not alter plasma leptin concentrations in these mice. Taken together, these findings suggest that ablation of *Rnf213* may mitigate the diabetic phenotype by preserving β cell function.

Amelioration by *Rnf213* ablation contradicts a mechanistic link between MMD and diabetes [8], if variants were associated with MMD by loss-of-function or haploinsufficiency of *RNF213*. Alterna-

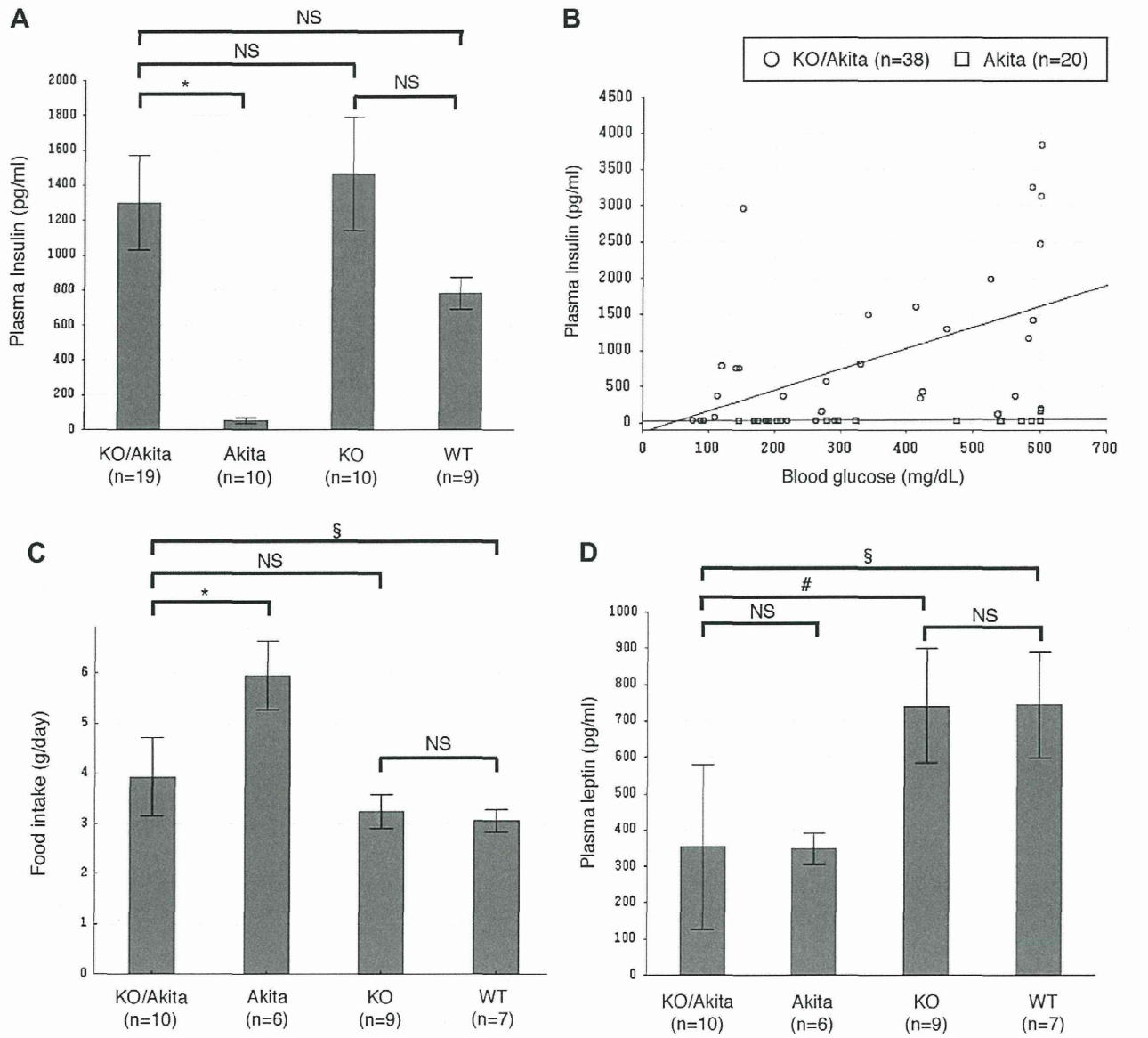

Fig. 3. Plasma insulin and leptin concentrations and food intake at 18 weeks of age. (A) Plasma insulin concentrations in KO/Akita, Akita, KO, and WT mice after a 6 h fast. Data are shown as mean ± SE. (B) Correlation between blood glucose and plasma insulin concentrations of KO/Akita and Akita mice after fasting for 6 h and 16 h (combined). (C) Food intake by KO/Akita, Akita, KO, and WT mice. (D) Plasma leptin concentrations of KO/Akita, Akita, KO, and WT mice after 16 h fasting. Data are shown as mean ± SD except for plasma insulin concentrations. $^{*}p < 0.05$ vs Akita, $^{\#}p < 0.05$ vs KO, $^{\S}p < 0.05$ vs WT, NS, not significant.

tively, pathological variants including R4810K of *RNF213* may cause MMD and diabetes by a gain-of-function or in a dominant-negative fashion. Among MMD predisposing diseases, diabetogenic mechanisms are well defined in MOPDII, a rare genetic disease characterized by severe growth retardation and early onset diabetes, as well as complication by MMD. Pericentrin, the causative gene for MOPDII, may regulate the intracellular distribution and secretion of insulin, and mutations of pericentrin may result in β-cell dysfunction [20]. The findings presented here indicate that β-cell dysfunction may have a mechanistic link with MMD.

Akita mice carrying a heterozygous C96Y mutation in the *Ins2* gene spontaneously develop hyperglycemia at an early age with reduced pancreatic β cell mass [12,13]. This C96Y mutation causes a conformational change in the insulin molecule, resulting in ER stress. ER stress, in turn, induces an unfolded protein response (UPR), indicating increased degradation of unfolded proteins by ER-associated degradation (ERAD), which is associated with E3 ligase and AAA + ATPase.

Recent studies [21,22] have demonstrated that the $Ins2^{C96Y}$ allele acts dominantly to enhance degradation of both the Akita and wild-type allele proinsulins by the ERAD pathway. We hypothesize that ablation of *Rnf213* may impair ERAD and lead to the sparing of wild-type proinsulin. Then we should explain how such preserved insulin secretion in KO/Akita mice reduced ER stress, as indicated by a reduction in the relative abundance of CHOP positive cells in these mice. Diabetes progresses more rapidly in male than female Akita mice [12]. This gender difference in susceptibility can be reversed by castration of males, thus suppressing hyperphagia [16]. Hyperphagia increases insulin demand due to elevated energy uptake, resulting in enhanced ER-stress with stimulated production of $Ins2^{C96Y}$. Such a vicious cycle may likely accelerate the progression of diabetes in male Akita mice. We found that

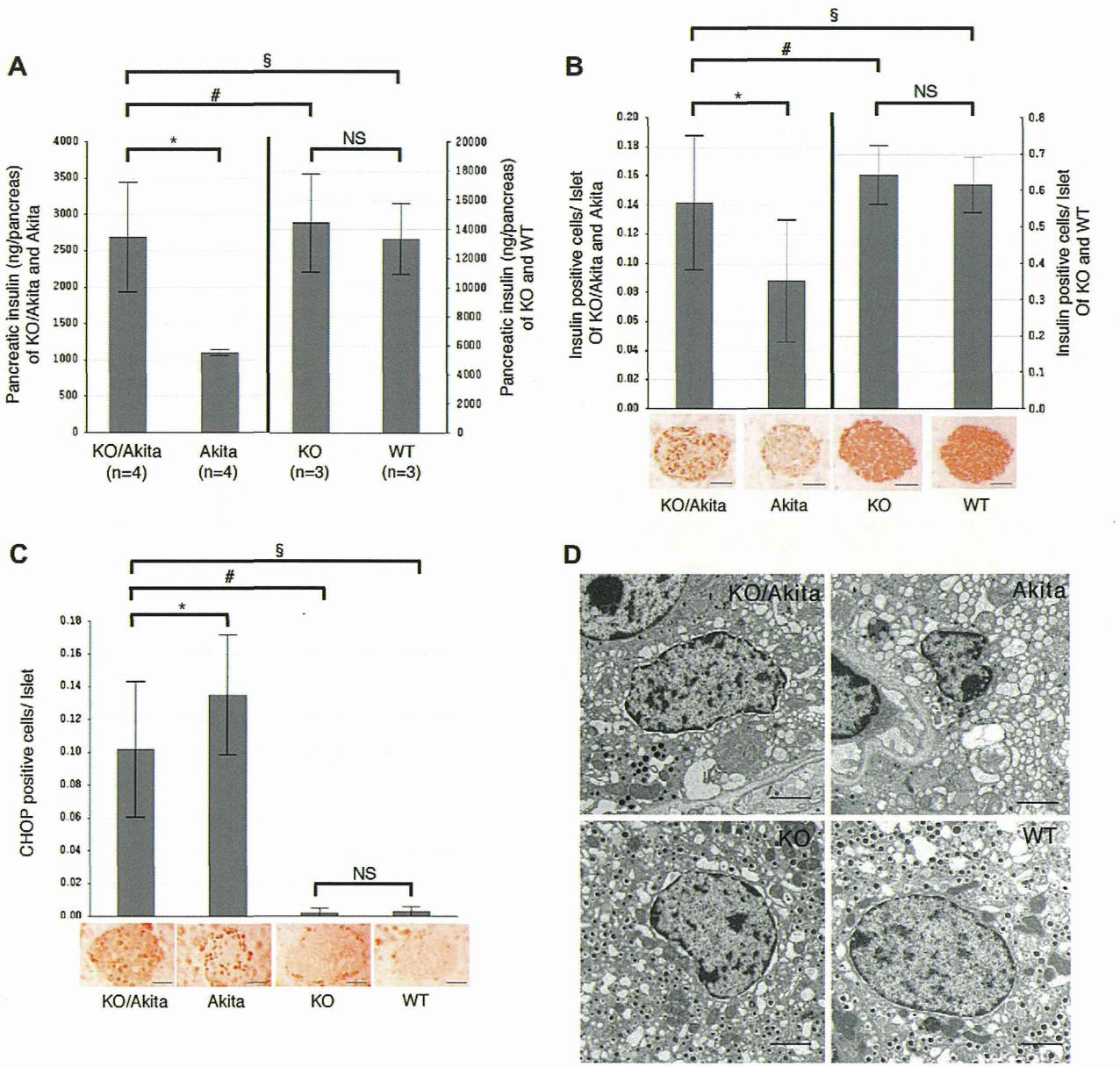

Fig. 4. Pancreatic insulin contents, insulin and CHOP immunohistochemistry, and electron microscopy of 18 week old mice. (A) Pancreatic insulin contents of KO/Akita, Akita, KO, and WT mice. (B) Representative images of islets stained with anti-insulin antibody (lower) and insulin positive cells per islet (upper) of KO/Akita ($n = 4$), Akita ($n = 4$), KO ($n = 3$), and WT ($n = 3$) mice. Quantification was performed on more than 20 islets from each mouse. Scale bar indicates 50 μm. (C) Representative images of islets stained with anti-CHOP antibody (lower) and CHOP positive cells per islet (upper) of KO/Akita ($n = 4$), Akita ($n = 4$), KO ($n = 3$), and WT ($n = 3$) mice. Quantification was performed on more than 20 islets from each mouse. Scale bar indicates 50 μm. (D) Electron micrographs of islets of KO/Akita, Akita, KO, and WT mice. Scale bar indicates 2 μm. Data are shown as mean ± SD. $^{*}p < 0.05$ vs Akita, $^{\#}p < 0.05$ vs KO, $^{\S}p < 0.05$ vs WT, NS, Not significant.

the higher serum insulin levels in KO/Akita mice were sufficient to suppress hyperphagia. Thus, *RNF213* ablation can spare wild-type insulin, thereby ameliorating this viscous cycle. Further study is warranted to test whether *RNF213* is involved in the ERAD pathway.

RNF213 is a single protein with two types of enzymatic activity, E3 ligase and AAA + ATPase [9]. AAA + ATPase is involved in various cellular processes, including vesicular transport, UPR, motor proteins and microtubule severing [11]. The association between *Rnf213* and β cell function is likely mediated by both E3 ligase and AAA + ATPase activities. The core assumption, that the normal allele of *Ins2* is also a target of degradation by ERAD, is intriguing and requires more quantitative assessment in the future. Future studies may help provide clues into a new therapeutic approach for diabetes as well as to gain insight into *RNF213* function.

Acknowledgments

This study was mainly supported by grants from the Ministry of Education, Culture, Sports, Science and Technology of Japan (Kiban Kenkyu A: 22249020) and from the Ministry of Health, Labour and Welfare of Japan (H23-Nanji-Ippan-01 and H23-Bio-Ippan-003) to AK and partially by grants from the Ministry of Education, Culture, Sports, Science and Technology of Japan (Tokubetukenkyuin

Syoreihi: 225192) to HK. We thank Ms. Emi Nakai for assistance with ES screening.

Appendix A. Supplementary data

Supplementary data associated with this article can be found, in the online version, at http://dx.doi.org/10.1016/j.bbrc.2013.02.015.

References

[1] J. Suzuki, A. Takaku, Cerebrovascular "moyamoya" disease. Disease showing abnormal net-like vessels in base of brain, Arch. Neurol. 20 (1969) 288–299.
[2] R.M. Scott, E.R. Smith, Moyamoya disease and moyamoya syndrome, N. Engl. J. Med. 360 (2009) 1226–1237.
[3] D.S. Kainth, S.A. Chaudhry, H.S. Kainth, F.K. Suri, A.I. Qureshi, Prevalence and characteristics of concurrent down syndrome in patients with moyamoya disease, Neurosurgery 72 (2013) 210–215.
[4] K. Okazaki, A. Kakita, H. Tanaka, K. Kimura, M. Minagawa, T. Morita, H. Takahashi, Widespread ischemic brain lesions caused by vasculopathy associated with neurofibromatosis type 1, Neuropathology 30 (2010) 627–633.
[5] M.B. Bober, N. Khan, J. Kaplan, K. Lewis, J.A. Feinstein, C.I. Scott Jr., G.K. Steinberg, Majewski osteodysplastic primordial dwarfism type II (MOPD II): expanding the vascular phenotype, Am. J. Med. Genet. A 152A (2010) 960–965.
[6] A.J. Anwar, J.D. Walker, B.M. Frier, Type 1 diabetes mellitus and Down's syndrome: prevalence, management and diabetic complications, Diabet. Med. 15 (1998) 160–163.
[7] M. Kamoun, N. Charfi, N. Rekik, M.F. Mnif, F. Mnif, H. Kmiha, Z. Mnif, M. Abid, Neurofibromatosis and Type 1 diabetes mellitus: an unusual association, Diabet. Med. 26 (2009) 1180–1181.
[8] R.S. Bower, G.W. Mallory, M. Nwojo, F.B. Meyer, Y.C. Kudva, Diabetes mellitus and the moyamoya syndrome, Ann. Intern. Med. 157 (2012) 387–388.
[9] W. Liu, D. Morito, S. Takashima, Y. Mineharu, H. Kobayashi, T. Hitomi, H. Hashikata, N. Matsuura, S. Yamazaki, A. Toyoda, K. Kikuta, Y. Takagi, K.H. Harada, A. Fujiyama, R. Herzig, B. Krischek, L. Zou, J.E. Kim, M. Kitakaze, S. Miyamoto, K. Nagata, N. Hashimoto, A. Koizumi, Identification of RNF213 as a susceptibility gene for moyamoya disease and its possible role in vascular development, PLoS One 6 (2011) e22542.
[10] R.J. Deshaies, C.A. Joazeiro, RING domain E3 ubiquitin ligases, Annu. Rev. Biochem. 78 (2009) 399–434.
[11] S.R. White, B. Lauring, AAA + ATPases: achieving diversity of function with conserved machinery, Traffic 8 (2007) 1657–1667.
[12] M. Yoshioka, T. Kayo, T. Ikeda, A. Koizumi, A novel locus, Mody4, distal to D7Mit189 on chromosome 7 determines early-onset NIDDM in nonobese C57BL/6 (Akita) mutant mice, Diabetes 46 (1997) 887–894.
[13] J. Wang, T. Takeuchi, S. Tanaka, S.K. Kubo, T. Kayo, D. Lu, K. Takata, A. Koizumi, T. Izumi, A mutation in the insulin 2 gene induces diabetes with severe pancreatic beta-cell dysfunction in the Mody mouse, J. Clin. Invest. 103 (1999) 27–37.
[14] J. Nozaki, H. Kubota, H. Yoshida, M. Naitoh, J. Goji, T. Yoshinaga, K. Mori, A. Koizumi, K. Nagata, The endoplasmic reticulum stress response is stimulated through the continuous activation of transcription factors ATF6 and XBP1 in Ins2^{+}/Akita pancreatic beta cells, Genes Cells 9 (2004) 261–270.
[15] J. Miyazaki, K. Araki, E. Yamato, H. Ikegami, T. Asano, Y. Shibasaki, Y. Oka, K. Yamamura, Establishment of a pancreatic beta cell line that retains glucose-inducible insulin secretion: special reference to expression of glucose transporter isoforms, Endocrinology 127 (1990) 126–132.
[16] M. Toyoshima, A. Asakawa, M. Fujimiya, K. Inoue, S. Inoue, M. Kinboshi, A. Koizumi, Dimorphic gene expression patterns of anorexigenic and orexigenic peptides in hypothalamus account male and female hyperphagia in Akita type 1 diabetic mice, Biochem. Biophys. Res. Commun. 352 (2007) 703–708.
[17] M.S. Martin-Gronert, S.E. Ozanne, Metabolic programming of insulin action and secretion, Diabetes Obes. Metab. 14 (Suppl. 3) (2012) 29–39.
[18] S.J. Marciniak, C.Y. Yun, S. Oyadomari, I. Novoa, Y. Zhang, R. Jungreis, K. Nagata, H.P. Harding, D. Ron, CHOP induces death by promoting protein synthesis and oxidation in the stressed endoplasmic reticulum, Genes Dev. 18 (2004) 3066–3077.
[19] S. Yamane, Y. Hamamoto, S. Harashima, N. Harada, A. Hamasaki, K. Toyoda, K. Fujita, E. Joo, Y. Seino, N. Inagaki, GLP-1 receptor agonist attenuates endoplasmic reticulum stress-mediated β-cell damage in Akita mice, J. Diabetes Invest. 2 (2011) 104–110.
[20] A. Jurczyk, S.C. Pino, B. O'Sullivan-Murphy, M. Addorio, E.A. Lidstone, P. Diiorio, K.L. Lipson, C. Standley, K. Fogarty, L. Lifshitz, F. Urano, J.P. Mordes, D.L. Greiner, A.A. Rossini, R. Bortell, A novel role for the centrosomal protein, pericentrin, in regulation of insulin secretory vesicle docking in mouse pancreatic beta-cells, PLoS One 5 (2010) e11812.
[21] J.R. Allen, L.X. Nguyen, K.E. Sargent, K.L. Lipson, A. Hackett, F. Urano, High ER stress in beta-cells stimulates intracellular degradation of misfolded insulin, Biochem. Biophys. Res. Commun. 324 (2004) 166–170.
[22] M. Liu, I. Hodish, C.J. Rhodes, P. Arvan, Proinsulin maturation, misfolding, and proteotoxicity, Proc. Natl. Acad. Sci. USA 104 (2007) 15841–15846.

Am J Physiol Heart Circ Physiol 305: H1658–H1667, 2013.
First published September 16, 2013; doi:10.1152/ajpheart.00349.2013.

A novel heart failure mice model of hypertensive heart disease by angiotensin II infusion, nephrectomy, and salt loading

Yasumasa Tsukamoto,[1,2] Toshiaki Mano,[1,2] Yasushi Sakata,[1] Tomohito Ohtani,[1] Yasuharu Takeda,[1] Shunsuke Tamaki,[1,2] Yosuke Omori,[1,2] Yukitoshi Ikeya,[1,3] Yuki Saito,[1,3] Ryohei Ishii,[4] Mitsuru Higashimori,[4] Makoto Kaneko,[4] Takeshi Miwa,[2] Kazuhiro Yamamoto,[5] and Issei Komuro[1]

[1]*Department of Cardiovascular Medicine, Osaka University Graduate School of Medicine, Suita, Japan;* [2]*Genome Information Research Center, Osaka University, Suita, Japan;* [3]*Division of Cardiology, Department of Internal Medicine, Nihon University School of Medicine, Tokyo, Japan;* [4]*Department of Mechanical Engineering, Osaka University, Suita, Japan; and* [5]*Department of Molecular Medicine and Therapeutics, Faculty of Medicine, Tottori University, Yonago, Japan*

Submitted 24 April 2013; accepted in final form 13 September 2013

Tsukamoto Y, Mano T, Sakata Y, Ohtani T, Takeda Y, Tamaki S, Omori Y, Ikeya Y, Saito Y, Ishii R, Higashimori M, Kaneko M, Miwa T, Yamamoto K, Komuro I. A novel heart failure mice model of hypertensive heart disease by angiotensin II infusion, nephrectomy, and salt loading. *Am J Physiol Heart Circ Physiol* 305: H1658–H1667, 2013. First published September 16, 2013; doi:10.1152/ajpheart.00349.2013.—Although the mouse heart failure (HF) model of hypertensive heart disease (HHD) is useful to investigate the pathophysiology and new therapeutic targets for HHD, the model using simple experimental procedures and stable phenotypes has not been established. This study aimed to develop a novel mouse HF model of HHD by combining salt loading and uninephrectomy with ANG II infusion. Eight-week-old C57BL/6 male mice were treated with ANG II infusion (AT), ANG II infusion and uninephrectomy (AN), ANG II infusion and salt loading (AS), or ANG II infusion, uninephrectomy, and salt loading (ANS). Systolic blood pressure was significantly elevated and left ventricular (LV) hypertrophy was found in AT, AN, AS, and ANS mice, and there were no significant differences in those parameters between the four groups. At 6 wk after the procedures, only ANS mice showed significant decreases in LV fractional shortening and increases in lung weight with a high incidence. This phenotype was reproducible, and there were few perioperative or early deaths in the experimental procedures. Severe LV fibrosis was found in ANS mice. Oxidative stress was enhanced and small GTPase Rac1 activity was upregulated in the hearts of ANS mice. After the addition of salt loading and uninephrectomy to the ANG II infusion mouse model, cardiac function was significantly impaired, and mice developed HF. This might be a novel and useful mouse HF model to study the transition from compensated LV hypertrophy to HF in HHD.

heart failure; mouse model; angiotensin II; renal dysfunction; salt loading; hypertensive heart disease

HYPERTENSIVE HEART DISEASE (HHD) is a major public health problem that contributes to cardiovascular morbidity and mortality. HHD patients with persistent pressure overload often demonstrate a transition from a phase of compensated hypertrophy to heart failure (HF). However, the mechanism of this transition is still unclear.

Animal models of HF have contributed greatly to the development of novel HF therapies or the elucidation of pathophysiology of HHD. Several animal models that mimic features of HHD have been used over the years (15). Large animal or rat models, such as the renal wrap dog model (11), spontaneously hypertensive rat (36), and Dahl salt-sensitive rat (4), have been generally used as models of HHD. Mice with genetic modification are valuable tools to study the mechanisms of various cardiovascular diseases. The C57BL/6 mouse strain serves as the genetic background of many transgenic and gene knockout models to validate the function of specific genes. Previous studies (10, 12, 49) have shown that ANG II infusion mouse models develop HHD with cardiac hypertrophy and fibrosis, but C57BL/6 mice infused with high doses of ANG II maintain cardiac function and do not develop HF (10, 12, 49). The transverse aortic constriction (TAC) model has been used for a mouse model of pressure overload (26), but it does not entirely mimic human HHD, and it is also difficult to prepare the model because microsurgical skills are required. Thus, there are few appropriate mouse models of HHD that mimic clinical HHD well and develop HF.

It is well known that chronic kidney disease (CKD) increases the risk of cardiovascular events and overall deaths (6) and is associated with HHD. It has been reported that uninephrectomy induces renal dysfunction, especially under the high-salt condition, in animal models (2, 38), although it is controversial whether uninephrectomy itself is generally a risk factor for CKD in humans (16, 47). High salt intake is also associated with the occurrence of hypertension (7) and significantly increases the risk of total cardiovascular disease (44).

In the present study, we sought to establish a new model of HHD in C57BL/6 mice by combining salt loading, uninephrectomy, and chronic ANG II infusion.

METHODS

This study conformed with the guiding principles of and was approved by Osaka University Graduate School of Medicine with regard to animal care and conformed with the National Institutes of Health (NIH) *Guide for the Care and Use of Laboratory Animals.*

Animal procedures. The procedures used for the different groups are shown in Table 1. Eight-week-old male C57BL/6 mice (Japan SLC, Shizuoka, Japan) were anesthetized with a mixture of ketamine HCl (80 mg/kg ip) and xylazine HCl (10 mg/kg ip). Mice were divided into the following groups: control, ANG II infusion (AT group), ANG II infusion and uninephrectomy (AN group), ANG II infusion and salt loading (AS group), and ANG II infusion, uninephrectomy, and salt loading (ANS group). The left kidneys of ANS and AN mice were removed through a flank incision (uninephrectomy). Control, AT, and AS mice underwent sham surgery by exposing the left kidney without removal. AT, AN, AS, and ANS mice were infused with ANG II (1.2 mg·kg^{-1}·day^{-1}, Sigma-Aldrich) by subcu-

Address for reprint requests and other correspondence: T. Mano, Dept. of Cardiovascular Medicine, Osaka Univ. Graduate School of Medicine, 2-2 Yamadaoka, Suita 565-0871, Japan (e-mail: mano@medone.med.osaka-u.ac.jp).

Table 1. *Procedures of the mouse model*

	Control Group	AT Group	AN Group	AS Group	ANS Group
ANG II infusion	−	+	+	+	+
Uninephrectomy	−	−	+	−	+
Salt loading (1% NaCl in drinking water)	−	−	−	+	+

Mice were divided into the following groups: control, ANG II infusion (AT group), ANG II infusion and uninephrectomy (AN group), ANG II infusion and salt loading (AS group), and ANG II infusion, uninephrectomy, and salt loading (ANS group).

taneous implantation of an osmotic minipump (Alza) immediately after the uninephrectomy/sham procedure. ANG II was dissolved in 0.01 mol/l acetic acid-saline. Osmotic minipumps containing 0.01 mol/l acetic acid-saline were implanted in control mice. After the procedures, AS and ANS mice were given drinking water containing 1% NaCl. All mice were fed a normal salt diet (rodent chow containing 0.3% NaCl). The diet and tap water were provided ad libitum throughout the experiment.

After the surgery, conscious systolic blood pressure (SBP) was monitored weekly with a tail-cuff system (BP-98A, Softron, Tokyo, Japan). Mice were analyzed 6 wk after surgery.

Echocardiography in mice. For the evaluation of cardiac dimension and contractility, a transthoracic echocardiographic experiment was performed on conscious mice using an echocardiographic machine equipped with a 25-MHz linear probe (Vevo 770, Visual Sonics), as previously described (25).

Tissue and blood sampling in mice. After echocardiography, mice were anesthetized with an intraperitoneal injection of ketamine and xylazine (100 and 10 mg/kg, respectively). Blood was collected from the inferior vena cava. The serum creatinine concentration was measured by an enzymatic method (21). The heart and lung were rapidly harvested, and the left ventricle (LV) and lung were weighed. LV and lung weight were corrected for tibial length. The apical part of the LV myocardium was snap frozen in liquid nitrogen and stored at −80°C for 2 wk before measurement of mRNA and Rac1 activities. Samples for immunohistochemistry were embedded in Tissue-Tek OCT compound (Sakura Finetechnical, Tokyo, Japan) and frozen. The rest of the LV and lung samples were fixed with phosphate-buffered 10% formalin solution for 48 h. Specimens were embedded in paraffin for histological analyses, 2-μm-thick sections of the lungs were stained with hematoxylin and eosin for routine histological examination, and 2 μm-thick transverse sections of the LV were stained with Sirius red for the detection of fibrosis (33). A whole LV transverse section image was made of 30–40 color ×100 magnification images using a digital microscopy and software (BZ-8000, Keyence, Osaka, Japan), and the ratio of the interstitial fibrosis area to myocardial area in a whole LV section was calculated. Fibrosis of the perivascular, epicardial, and endocardial areas was excluded from the analysis. TRITC-labeled lectin from *Triticum vulgaris* (Sigma) was used for membrane staining (31). Sections were analyzed with fluorescent digital microscopy (BZ-8000, Keyence). Suitable cross-sections of cardiomyocytes for the area measurements were defined as having round to oval membrane staining from which the area was calculated. The fibrosis area, myocardial area, and cross-sectional area of cardiomyocytes were measured using NIH ImageJ 1.43u software.

Hemodynamic analysis. Mice that survived over 35 days after surgery were assessed for open-chest approach hemodynamic measurements as previously described (13, 34, 45). Anesthesia was induced with 3% followed by 1.5% isoflurane once the mice were intubated. The adequacy of anesthesia was monitored by the stability of blood pressure, heart rate, and lack of flexor responses to a paw pinch. A Millar 1.0-Fr high-fidelity manometer-tipped catheter (SPR-1000) was inserted into the LV after a stab of the apex with a 26-gauge needle through the stab wound to record LV pressure to determine the LV end-diastolic pressure (LVEDP), peak positive rate of LV pressure development (+dP/dt), and time constant of LV relaxation (τ).

Measurement of LV myocardial stiffness in mice. We evaluated LV myocardial stiffness at 4 wk after surgery with a balloon-type sensing system as previously described (17, 45). Skinned LV muscles from mice were prepared according to previously reported methods (46). The skinned transverse section was placed around a latex balloon (Labo Support) while the pressure inside the balloon was monitored. The balloon was then dilated with the deformation information of the balloon and the specimen captured by a charge-coupled device camera. Young's modulus (E_H) was obtained from the internal pressure of the balloon and the strain of the transverse LV section based on a dual-cylinder model.

Measurements of mRNA levels. Total RNA was extracted from LV tissue and reverse transcribed to cDNA as previously described (50). Quantitative real-time RT-PCR with the ABI PRISM 7900 HT Sequence Detection System and software (Applied Biosystems, Foster City, CA) was conducted to measure mRNA levels of β-actin, atrial natriuretic peptide (ANP), brain natriuretic peptide (BNP), collagen type Iα, and connective tissue growth factor (CTGF). The sequence of the primers and Taqman probes for BNP and CTGF have been previously described (5, 19). The primers and Taqman probes for β-actin, ANP, and collagen type Iα were assays-on-demand gene expression products (assay identifiers: Mm00607939_s1, Mm01255748_g1, and Mm00801666_g1, respectively, Applied Biosystems). The amount of each mRNA was divided by β-actin mRNA to correct the efficiency of cDNA synthesis and normalized to the mean of the control.

Immunohistochemistry for 4-hydroxy-2-nonenal protein expression. The expression of 4-hydroxy-2-nonenal (4-HNE), a byproduct of lipid peroxidation and an indicator for oxidative stress, was determined by immunohistochemical staining. Cryostat transverse sections were stained with mouse monoclonal anti-4-HNE antibody (1:50 dilution, NOF Medical Department, Tokyo, Japan) as previously described (30) using the mouse on mouse system (Nichirei Bioscience, Tokyo, Japan). The area and intensity of staining for HNE were blinded to the score for semi-quantification (32). The scoring range was defined as as follows: *0* = no visible staining, *1* = faint staining, *2* = moderate staining, *3* = strong staining, and *4* = very strong staining. Scores were determined by three independent observers blinded for the identification of the mice and were averaged.

In vitro experiments in cultured cardiomyocytes. Neonatal rat cardiac ventricular myocytes were isolated using standard techniques from Wistar rats with modifications of previously described methods (9, 29). Cardiomyocytes were suspended in 50% DMEM (Invitrogen) plus 50% medium 199 (M199; Invitrogen) supplemented with 10% FCS (Invitrogen). Cells were allowed to attach for 24 h. The medium was replaced with serum-free 50% DMEM plus 50% M199 (referred to as "control medium"), and cells were incubated for an additional 24 h. To assess the effects of high salt and ANG II, cardiomyocytes were incubated with high-salt medium (Na^+ concentration of 162 mmol/l) or ANG II (1 μmol/l, Sigma) for 3 h. The high-salt medium was made by simply adding NaCl. Cardiomyocytes with control medium (Na^+ concentration of 150 mmol/l) were used as controls. Cellular protein content was quantified by a modified Lowry assay.

Measurement of Rac1 activities. Activated Rac1 was analyzed by the p21-binding domain of a p21-activated protein kinase 1 pulldown assay with a commercially available kit (Rac1 Activation Assay Kit, Cell Biolabs, San Diego, CA) according to the manufacturer's protocol (41).

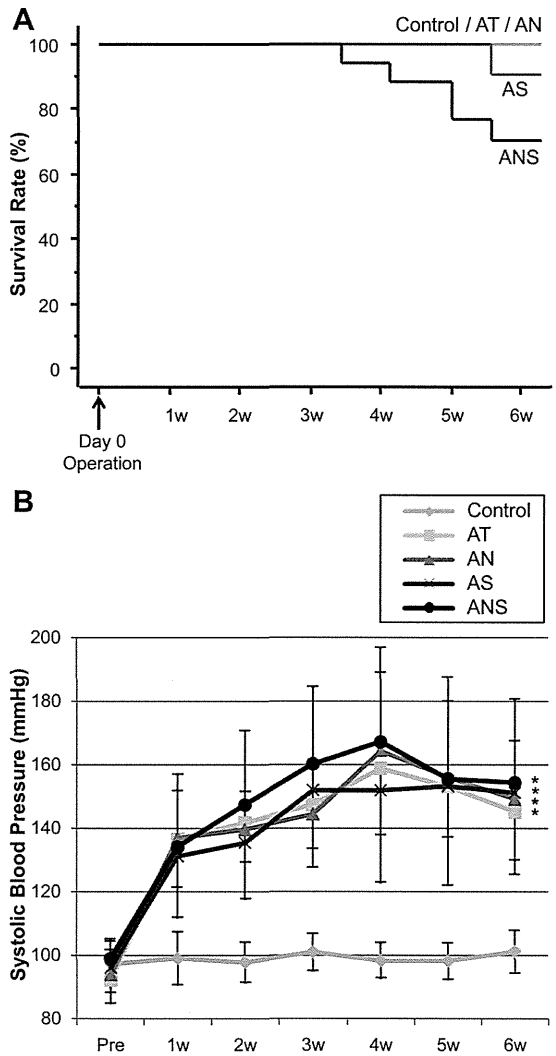

Fig. 1. Survival curves and systolic blood pressure (SBP) in the mouse model. *A*: survival curves of control, ANG II infusion (AT), ANG II infusion and uninephrectomy (AN), ANG II infusion and salt loading (AS), and ANG II infusion, uninephrectomy, and salt loading (ANS) mouse groups after the procedures. *B*: SBP values of the five groups over the time course of the experiment. Values are means ± SD. *$P < 0.05$ vs. the control group.

Statistical analysis. Data are presented as means ± SD and were analyzed using statistical software (STATVIEW version 5.0, SAS Institute, Cary, NC). Multiple-group comparison was performed by one-way ANOVA followed by the Tukey-Kramer method for comparison of means. The time course of SBP among multiple groups was assessed using repeated-measures ANOVA followed by the Tukey's test. Comparisons between two groups were analyzed by an unpaired *t*-test. *P* values of <0.05 were considered statistically significant.

RESULTS

Mortality in mouse models. Survival curves of mice are shown in Fig. 1*A*. Mortality rates until 6 wk after surgery in control, AT, AN, AS, and ANS mice were 0%, 0%, 0%, 9.1%, and 35.3%, respectively. Significant LV dilatation and increases of lung weight were observed in all dead AS and ANS mice at necropsies. ANS mice demonstrated high mortality, which could be attributed to HF.

Physiological parameters and renal function in mouse models. The results of physiological and biochemical parameters at 6 wk after surgery are shown in Table 2, and a time course of SBP is shown in Fig. 1*B*. AT, AN, AS, and ANS mice showed significantly higher SBPs than control mice, whereas there were no significant differences in SBP among the four groups. The serum creatinine concentration was significantly higher in AN and ANS mice than in non-nephrectomized mice. This result indicates that renal dysfunction occurred in mice with uninephrectomy and ANG II infusion. Serum Na^+ levels were higher in ANS mice than in control and AT mice.

ANS mice developed HF. At 6 wk after the operation, the increase in LV end-diastolic posterior wall thickness was found to be similar in AT, AN, AS, and ANS mice compared with control mice (Fig. 2*D*). LV weight/tibial lengh was increased in AT, AN, AS, and ANS mice compared with control mice (Fig. 3*A*). Histological examination also revealed an increase in the cross-sectional area of cardiomyocytes in AT, AN, AS, and ANS mice compared with control mice (Fig. 3*D*). These parameters indicate that hypertrophy of cardiomyocytes occurred similarly in AT, AN, AS, and ANS mice. LV endocardial fractional shortening was depressed in ANS mice compared with any other group mice at 6 wk after surgery (Fig. 2*C*). The LV end-diastolic diameter of ANS mice was enlarged compared with AT, AN, and AS mice (Fig. 2*B*). ANS mice did not show LV systolic dysfunction or overt HF at 4 wk after the operation. At 5 wk after the operation, ANS mice showed LV systolic dysfunction, and 25% of ANS mice manifested congestive HF as assessed by the increase in lung weight (Table 3). An index of LV myocardial stiffness, E_H, was increased in ANS mice at 4 wk after surgery (Fig. 4*A*). LVEDP was significantly increased and LV $+dP/dt$ was decreased at 6 wk after surgery in ANS mice compared with control mice (Fig. 4*B*). τ was prolonged in ANS mice (Fig. 4*B*). These results showed that LV systolic and diastolic function were impaired in ANS mice. Lung weights were not changed in AT, AN, and AS mice

Table 2. *Physiological and biochemical parameters at 6 wk after surgery in the mouse model*

	Control Group	AT Group	AN Group	AS Group	ANS Group
Number of mice/group	12	9	10	10	11
Body weight, g	28.1 ± 1.6	26.6 ± 1.4	25.7 ± 1.7*	25.0 ± 1.3*	24.9 ± 1.7*
Tibial length mm	18.2 ± 0.3	18.2 ± 0.2	18.2 ± 0.3	18.2 ± 0.2	18.0 ± 0.2
Systolic blood pressure, mmHg	101 ± 7	145 ± 18*	149 ± 24*	151 ± 18*	154 ± 17*
Heart rate, beats/min	678 ± 67	693 ± 58	639 ± 79	701 ± 43	710 ± 52
Serum creatinine, mg/dl	0.09 ± 0.02	0.13 ± 0.03	0.20 ± 0.06*†	0.14 ± 0.04	0.20 ± 0.05*†‡
Serum Na^+, meq/l	150 ± 2.3	150 ± 1.8	153 ± 3.6	154 ± 1.7	156 ± 4.5*†

Results are means ± SD. Biochemical parameters were analyzed from blood samples from 6–8 mice/group. *$P < 0.05$ vs. the control group; †$P < 0.05$ vs. the AT group; ‡$P < 0.05$ vs. the AS group.

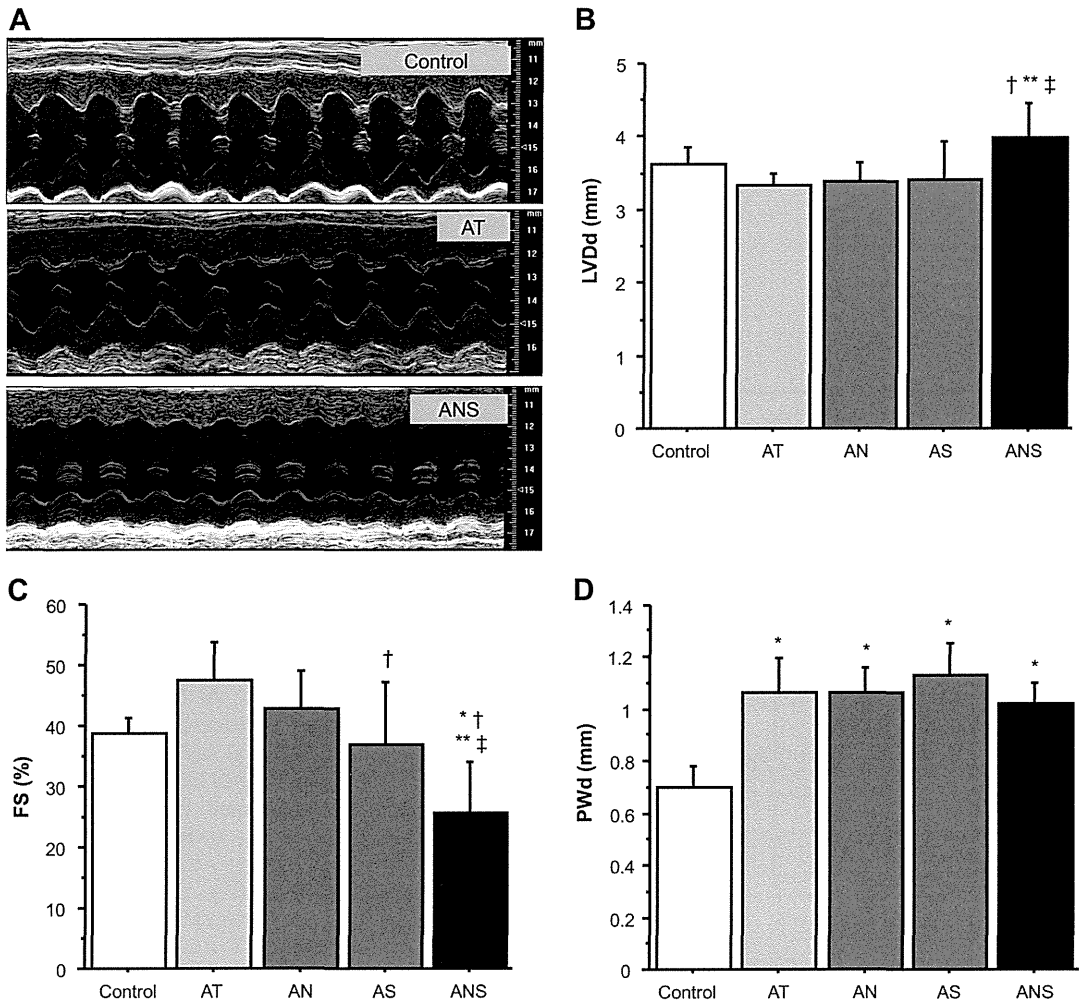

Fig. 2. Analysis with echocardiography at 6 wk after surgery in the mouse model. *A*: typical examples of M-mode echocardiograms. *B–D*: left ventricular (LV) diastolic dimension (LVDd; *B*), LV fractional shotening (FS; *C*), and end-diastolic wall thickness of the LV posterior wall (PWd; *D*) in control, AT, AN, AS, and ANS mice. $*P < 0.05$ vs. control mice; $\dagger P < 0.05$ vs. AT mice; $**P < 0.05$ vs. AN mice; $\ddagger P < 0.05$ vs. AS mice.

compared with control mice, but ANS mice showed a significant increase in lung weight compared with any other group of mice. Histological observation of the lung revealed severe pulmonary alveolar edema in ANS mice. These results are consistent with pulmonary congestion. Levels of ANP and BNP mRNA expression were significantly increased in AS and ANS mice compared with control and AT mice, suggesting that additive salt loading with ANG II infusion induced an upregulation of gene expression of ANP and BNP in the LV.

Reproducibility of the phenotype of ANS mice. From three independent experiments, the reproducibility of the phenotype of ANS mice was analyzed (Table 4). LV weight increased similarly in the three experiments. This suggests that the loading condition was stable in this model of HF. The mortality rate of each experiment was 20–42%, and all of the deaths occurred between 3 and 6 wk with signs of congestive HF. Early mortality, defined as death within 2 wk after the procedures, was 0% in ANS mice. The rate of HF in the surviving mice was 67–75%, which was defined as increases in lung weights.

LV fibrosis was found in ANS mice. LV interstitial fibrosis was observed in AN, AS, and ANS mice and was severe in ANS mice (Fig. 5, *A* and B). mRNA levels of collagen type Iα were also increased in the LVs of AN, AS, and ANS mice, and ANS mice showed greater levels compared with AN mice. CTGF levels were also increased in the LVs of ANS mice compared with control, AT, and AN mice (Fig. 5, *C* and *D*).

Oxidative stress was increased in ANS mouse hearts. To examine the extent of oxidative stress in the heart, the level of 4-HNE-modified protein was assessed in cardiac tissue using immunohistochemical staining with anti-4-HNE antibody as a marker of oxidative stress. 4-HNE-modified protein adducts in the LVs of ANS mice were increased significantly compared with any other group (Fig. 6, *A* and *B*).

Rac1 activity was upregulated in ANS mouse hearts and cardiomyocytes with high salt and ANG II. Rac1 activity was significantly increased in ANS mouse hearts but not in AT, AN, or AS mouse hearts (Fig. 7*A*). Rac1 activity was significantly increased in cardiomyocytes treated with both high salt and ANG II but was not significant in cardiomyocytes with only high salt or ANG II (Fig. 7*B*).